Research article

Tomáš Neuman*, Javier Aizpurua and Ruben Esteban

Quantum theory of surface-enhanced resonant Raman scattering (SERRS) of molecules in strongly coupled plasmon–exciton systems

https://doi.org/10.1515/nanoph-2019-0336
Received August 30, 2019; revised October 22, 2019; accepted October 26, 2019

Abstract: Localised surface plasmons can couple strongly with the electronic transitions of a molecule, inducing new hybridised states of light and matter, the plasmon–exciton polaritons. Furthermore, molecules support vibrational degrees of freedom that interact with the electronic levels, giving rise to inelastic resonant Raman scattering under coherent laser illumination. Here we show the influence of strong plasmon–exciton coupling on resonant Raman processes that populate the vibrational states of the molecule and that lead to the characteristic surface-enhanced Raman scattering spectra. We develop analytical expressions that give insight into these processes for the case of moderate illumination intensity, weak electron–vibration coupling and no dephasing. These expressions help us to elucidate the twofold role of plasmon–exciton polaritons to pump the system efficiently and to enhance the Raman emission. Our results show a close analogy with the optomechanical process described for off-resonant Raman scattering but with a difference in the resonant reservoir. We also use full numerical calculations to study the effects reaching beyond these approximations and discuss the interplay between the fluorescence background and the Raman lines. Our results allow for better understanding and exploitation of the strong coupling regime in vibrational puming and in the surface-enhanced resonant Raman scattering signal.

Keywords: strong coupling; Raman scattering; plasmonics; molecular optomechanics; SERRS.

1 Introduction

Metallic nanoparticles support plasmonic modes at optical frequencies than can confine the electromagnetic energy to effective volumes [1–6] even below ≈10–1000 nm^3 and thus give rise to efficient coupling of the particle plasmons with excitations in nearby molecules (e.g. molecular excitons). This efficient interaction has found, among others, a prominent application in surface-enhanced Raman scattering (SERS) [7–12], where the inelastic Raman signal containing the vibrational signature of the molecule is enhanced.

The dynamics of the SERS process has been recently described in a cavity Quantum Electrodynamics (QED) framework [5, 13–18]. In particular, it has been shown that in off-resonance SERS, where the electronic transitions of the molecules are strongly detuned with respect to the exciting laser, the underlying physics can be understood as a molecular optomechanical process [5, 14, 16–21], in which the vibration of the molecules and the plasmonic resonance replace the macroscopic mechanical vibrations and the optical mode in conventional optomechanics [22], respectively. This QED-based theory has described regimes of nonlinear SERS with the use of a single incident laser and has naturally addressed the effect of optomechanical vibrational pumping [23–27], a process where enhancement of the Stokes–Raman emission leads to population of the vibrational mode of the molecule.

On the other hand, in surface-enhanced resonant Raman scattering (SERRS), an electronic transition close to the energy of the exciting laser considerably affects the Raman process and gives rise to complex nonlinear phenomena [28]. In this case, it is possible to describe the

***Corresponding author: Tomáš Neuman,** Centro de Física de Materiales CFM–MPC, Centro Mixto CSIC-UPV/EHU, 20018 San Sebastián/Donostia, Basque Country, Spain,
e-mail: neumat@seznam.cz.
https://orcid.org/0000-0003-3089-5805
Javier Aizpurua: Centro de Física de Materiales CFM–MPC, Centro Mixto CSIC-UPV/EHU, 20018 San Sebastián/Donostia, Basque Country, Spain; and Donostia International Physics Center (DIPC), 20018 San Sebastián/Donostia, Basque Country, Spain
Ruben Esteban: Donostia International Physics Center (DIPC), 20018 San Sebastián/Donostia, Basque Country, Spain; and IKERBASQUE, Basque Foundation for Science, Maria Diaz de Haro 3, 48013 Bilbao, Basque Country, Spain

Open Access. © 2019 Tomáš Neuman et al., published by De Gruyter. This work is licensed under the Creative Commons Attribution 4.0 Public License.

Unauthenticated
Download Date | 12/20/19 6:11 PM

light–matter interaction by a similar Hamiltonian as the one used in hybrid optomechanics [13, 29, 30], where a two-level excitation is included in the system, leading to a nonlinear behaviour of the response.

The system is said to be in weak-coupling regime (or in the bad-cavity limit), when the interaction strength, g, between the plasmon and the electronic transition remains small in comparison with the plasmonic losses, γ_a (assuming negligible molecular losses and pure dephasing), i.e. $g \lesssim \gamma_a/2$. Under such conditions, the electronic transition in the molecule and the plasmon can be considered as well-defined excitations that interact weakly. We have addressed this situation in our previous work [28], where we also compare the model describing resonant Raman with the off-resonant Raman model.

On the other hand, if the coupling between the plasmon and the molecular electronic states is sufficiently large to overcome the plasmonic losses, i.e. $g \gtrsim \gamma_a/2$, the system reaches the regime of strong coupling and the electronic transition hybridises with the plasmon. Large enough values of g to achieve strong coupling are nowadays typically achieved by coupling plasmonic nanostructures with either J-aggregates [31–39], large complex dyes characterised by large dipole moments, or with a large number of small molecules forming a collective bright mode of larger effective coupling strength [40–44]. However, recently, it has become possible to achieve strong coupling even with a single small molecule or quantum dot [37, 42, 43, 45–47], opening new possibilities for fundamental studies of hybrid light–matter quantum states. The regime of strong coupling between a single two-level electronic transition and a plasmonic mode is characterised by a structure of energy levels forming the so-called Jaynes–Cummings (J-C) ladder, which leads to complicated patterns of inelastic resonance–fluorescence light emission [48, 49].

In this work, we present a theoretical study of vibrational pumping and Raman scattering in resonant SERS systems [50] in the framework of cavity QED, focusing on the regime of strong coupling between the single molecule and a plasmonic mode. After a brief introduction to the regime of strong coupling, we describe the resonant SERS Hamiltonian and develop a simplified, but intuitive, analytical approach that allows for understanding the physical mechanism of vibrational pumping and vibrational Raman scattering. Specifically, we assume a scenario where the illuminating laser is not too strong, the pure dephasing processes that broaden the electronic transitions are not considered, and the coupling between electronic and vibrational levels of the molecule is sufficiently weak so that the zero-phonon line dominates the fluorescence spectrum. In the second part of the article, we numerically solve the system's dynamics without simplifications to show successively how large electronic–vibrational coupling, pure dephasing, and intense laser illumination, effects that might be important in real experiments, affect the response of the system.

2 Plasmon–exciton strong coupling

Before discussing the SERS process, we briefly summarise the properties of a plasmonic system strongly coupled with an electronic transition. The system under consideration is sketched in Figure 1A, where a plasmonic structure resonant at energy $\hbar\omega_{\mathrm{pl}}$ interacts with a molecule, described as a two-level system (TLS) of excitation energy $\hbar\omega_{\mathrm{eg}}$.

This system can be described within the rotation wave approximation by the J-C Hamiltonian, and we thus refer in the following to the J-C system when discussing the coupling of the TLS and the plasmon in the absence of any vibration. The J-C Hamiltonian driven by a laser of frequency ω_{L} can be written as follows:

$$H_{\mathrm{J-C}} = \hbar\omega_{\mathrm{pl}} a^{\dagger}a + \hbar\omega_{\mathrm{eg}}\sigma^{\dagger}\sigma + \hbar g a^{\dagger}\sigma + \hbar g^{*} a\sigma^{\dagger} + \hbar\mathcal{E}a e^{i\omega_{\mathrm{L}}t} + \hbar\mathcal{E}^{*} a^{\dagger} e^{-i\omega_{\mathrm{L}}t}, \tag{1}$$

with $a(a^{\dagger})$, the annihilation (creation) bosonic operators associated to the plasmon; and $\sigma(\sigma^{\dagger})$, the TLS lowering (raising) operators. Here g is the plasmon–molecule coupling strength, and the pumping by the laser is introduced via the parameter $\mathcal{E}$, proportional to the amplitude of the electric field of the driving laser and to the transition dipole moment of the molecule. We further assume that both g and $\mathcal{E}$ are real. The explicit time dependence appearing in the pumping term is transformed out of the Hamiltonian by working in the standard interaction picture where the new Hamiltonian is obtained from the unitary transformation $H' = UHU^{\dagger} + i\hbar\dot{U}U^{\dagger}$, with $U = \exp(iH_{\mathrm{NI}}t)$, and $H_{\mathrm{NI}} = \hbar\omega_{\mathrm{L}}(a^{\dagger}a + \sigma^{\dagger}\sigma)$ is the noninteracting part of the Hamiltonian. In this picture, the explicit time dependence of the Hamiltonian drops out, the plasmon frequency is replaced by $\omega_{\mathrm{pl}} \to \Delta = \omega_{\mathrm{pl}} - \omega_{\mathrm{L}}$, and the molecule TLS frequency transforms analogously as $\omega_{\mathrm{eg}} \to \delta = \omega_{\mathrm{eg}} - \omega_{\mathrm{L}}$. For simplicity, throughout the article, we consider that the frequency of the molecular transition is exactly tuned to the plasmon frequency $\omega_{\mathrm{pl}} = \omega_{\mathrm{eg}}$ ($\Delta = \delta$).

Losses are added by using the master equations for the time evolution of the density matrix, ρ, and introducing Lindblad terms for the TLS, $\mathcal{L}_{\sigma}(\rho)$, and the plasmon, $\mathcal{L}_{a}(\rho)$,

Unauthenticated
Download Date | 12/20/19 6:11 PM

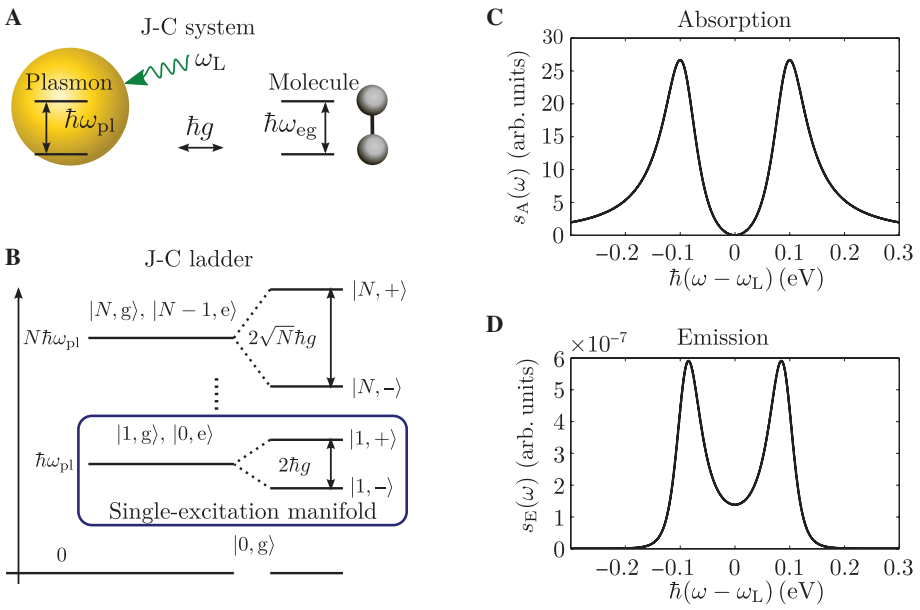

Figure 1: Strong coupling between a plasmonic system and an electronic transition of a molecule, in the absence of molecular vibrations. (A) Schematic depiction of the possible realisation of the Jaynes–Cummings (J-C) model. A dye molecule with an excitonic transition of energy $\hbar\omega_{eg}$ is placed near a metallic cavity that sustains a plasmonic mode at energy $\hbar\omega_{pl}$. Both systems are tuned to the resonant condition $\omega_{eg}=\omega_{pl}$. The plasmonic cavity is illuminated by a single pump laser of frequency, ω_L, or by a combination of a pump and a probe laser. (B) J-C ladder showing the coherent mixing of the electronic levels of the molecule with the bosonic levels of the plasmon (defined by states $|N, g(e)\rangle$ in the noninteracting case) into a set of hybrid states $|N,\pm\rangle$ under the strong-coupling conditions. The blue frame marks the single-excitation manifold determining the system response under weak-illumination conditions. (C) Absorption spectrum of a weakly perturbing probe for pumping amplitude $\hbar\mathcal{E}=1$ meV. The pump laser frequency is fixed to $\omega_L=\omega_{pl}$ ($\Delta=0$), and we change the frequency of the probe laser. (D) Emission spectrum of the J-C system for zero detuning of the laser $\omega_L=\omega_{pl}$ ($\Delta=0$) and pumping amplitude $\hbar\mathcal{E}=1$ meV. The plasmon–molecule interaction considered for the calculations corresponds to the strong-coupling regime and is described within the J-C model for the following values of the parameters: $\hbar\gamma_\sigma=2\times10^{-5}$ eV, $\hbar\gamma_a=150$ meV, $\hbar g=100$ meV, $\hbar\omega_{pl}=\hbar\omega_{eg}=\hbar\omega_L=2$ eV.

$$\mathcal{L}_\sigma(\rho)=-\frac{\gamma_\sigma}{2}(\{\sigma^\dagger\sigma,\rho\}-2\sigma\rho\sigma^\dagger), \tag{2}$$

$$\mathcal{L}_a(\rho)=-\frac{\gamma_a}{2}(\{a^\dagger a,\rho\}-2a\rho a^\dagger) \tag{3}$$

with γ_σ and γ_a, the corresponding loss rates of the exciton and plasmon, respectively, and $\{\cdot,\cdot\}$, the anticommutator. We neglect the effect of finite temperature (we consider $T=0$ K). The possibility of pure dephasing, leading to decoherence of the TLS without directly involving decay from the excited to the ground state, is considered in a later section.

To understand the behaviour of the system, we first briefly consider that the plasmon excitation is switched off. In this case, the system can be represented in the basis of states $|N, g(e)\rangle=|N\rangle\otimes|g(e)\rangle$ (with $\otimes$ the direct product), combining the plasmon number states $|N\rangle$ and the electronic ground (excited) state $|g(e)\rangle$ of the molecule. For $\omega_{eg}=\omega_{pl}$ and negligible interaction g, the states $|N-1, e\rangle$ and $|N, g\rangle$ are degenerate, and their energies form an equally spaced ladder (at the left of the scheme in Figure 1B). When g overcomes the system losses, the system enters the strong coupling regime where the degeneracy is lifted, resulting in a new set of hybrid polaritonic states $|N,+\rangle$ and $|N,-\rangle$ [$|N,\pm\rangle=(|N-1,e\rangle\pm|N,g\rangle)/\sqrt{2}$]. These states form a set of structured levels called the J-C ladder, which is sketched in Figure 1B to the right of the uncoupled $|N, g(e)\rangle$ levels. The energy splitting between these two states, $\Delta E_{J-C}(N)$, is proportional to the square root of the number of plasmonic excitations present in the system and to the coupling constant g via $\Delta E_{J-C}(N)=2\sqrt{N}\hbar g$. For this general discussion, we ignore that the losses can modify the exact splitting and coherent mixing of the bare states. For weak illumination, $N\ll1$, most transitions occur between the ground state and the so-called single-excitation manifold containing the states $|1,\pm\rangle$ (blue frame in Figure 1B), so that the absorption peaks appear at $\approx\omega_{pl}\pm g$.

To illustrate this behaviour, we first consider that the system is pumped by a laser at frequency ω_L in (1) and probed by a perturbative laser with frequency ω [note that the probe is not explicitly present in the Hamiltonian of (1)]. The system is strongly coupled with the parameters $\hbar g=100$ meV and $\hbar\gamma_a=150$ meV. We calculate the

Unauthenticated
Download Date | 12/20/19 6:11 PM

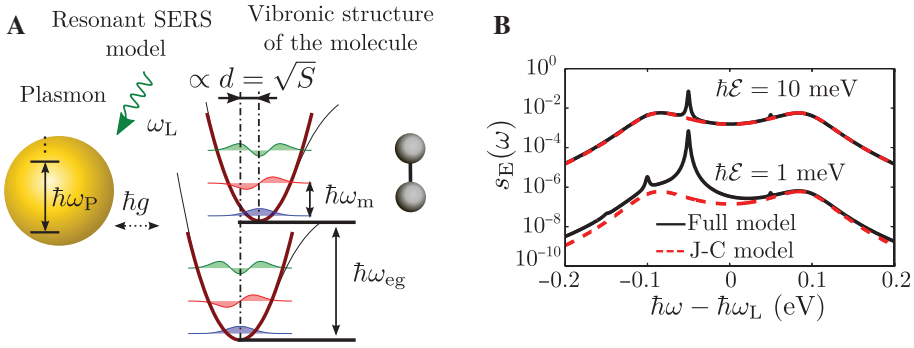

Figure 2: Schematics of the system considered for the description of SERRS alongside with examples of inelastic SERRS and Jaynes-Cummings spectra.
(A) Schematic depiction of the system where a plasmonic mode interacts with the electronic states of the molecule, which are further coupled to molecular vibrations. A dye molecule with an excitonic transition of energy $\hbar\omega_{eg}$ is placed into a plasmonic cavity that supports a resonance at energy $\hbar\omega_{pl}$ tuned to the molecular transition ($\hbar\omega_{pl} = \hbar\omega_{eg}$). Each molecular electronic level serves as a potential energy surface (PES) supporting a vibrational mode. The excited state and the ground state PES are mutually displaced as given by the dimensionless displacement d. The plasmon is illuminated by a single intense laser of frequency ω_L and pumping amplitude $\mathcal{E}$ that triggers the surface-enhanced Raman scattering process. (B) Two examples of emission spectra calculated using the full model where a vibrational mode is present (black lines) and the J-C model without considering the vibrations (red dashed line) calculated for $\hbar\mathcal{E} = 1$ meV and 10 meV, respectively. The spectra in (B) are calculated using the parameters for the J-C model as in Figure 1 and the following values for the vibrations: $\hbar\gamma_b = 2$ meV, $\hbar\omega_m = 50$ meV, and $\sqrt{S} = 0.1$.

absorption[1] as the Fourier transform of the two-time correlation function:

$$s_A(\omega) \propto -2\mathrm{Re}\int_0^\infty \langle [a^\dagger(0), a(\tau)]\rangle_{ss} e^{i\omega\tau} d\tau \approx 2\mathrm{Re}\int_0^\infty \langle a(\tau)a^\dagger(0)\rangle_{ss} e^{i\omega\tau} d\tau, \quad (4)$$

where $[\cdot,\cdot]$ denotes the commutator, and $\langle\cdot\rangle_{SS}$ is the steady-state mean value, which can be evaluated with help of the quantum regression theorem [51].

In Figure 1C, we plot $s_A(\omega)$ for a pumping amplitude $\hbar\mathcal{E} = 1$ meV that weakly populates the system. The results in Figure 1C are in good agreement with the expectation foreseen from the structure of the J-C ladder. The absorption spectrum consists of two absorption peaks separated by ≈ 200 meV $\approx 2\hbar g$ emerging from the transitions $|0, g\rangle \to |1, \pm\rangle$, in accordance with our discussion of the hybrid polaritonic states.

To facilitate the understanding of the following sections, we also briefly introduce the emission of the pumped J-C model. In this case, we excite the system with a monochromatic laser and study the emitted spectra given by the one-sided Fourier transform of the two-time correlation function:

$$s_E(\omega) \propto 2\mathrm{Re}\int_0^\infty [\langle a^\dagger(0)a(\tau)\rangle_{ss} - \langle a^\dagger(0)\rangle_{SS}\langle a(\tau)\rangle_{SS}] e^{i\omega\tau} d\tau. \quad (5)$$

We plot in Figure 1D the inelastic emission spectra (for clarity, we always subtract the elastic component) of the J-C system for a pumping amplitude $\hbar\mathcal{E} = 1$ meV and for $\hbar\omega_L = \hbar\omega_{pl} = \hbar\omega_{eg} = 2$ eV. The emission spectrum yields a double-peak structure originated from the incoherent decay of the polaritonic states to the ground state ($|1, \pm\rangle \to |0, g\rangle$).

Last, we emphasise that here we focus on the weak illumination regime, in which the laser moderately populates the polaritonic states ($N \ll 1$). For intense laser illumination, the optical absorption and light emission from a strongly coupled J-C system are nontrivial, as described in detail elsewhere [48, 52]. We briefly discuss this regime of strong illumination in a separate section at the end of this work.

3 Quantum description of SERRS in strong coupling

We model the plasmon-enhanced vibrational Raman processes as sketched in Figure 2A. We consider a single vibrational mode of the molecule that, in the harmonic approximation, is described as a bosonic excitation of angular frequency ω_m, with b ($b^\dagger$) its annihilation (creation) operators. The Hamiltonian of the uncoupled vibrations is

$$H_{vib} = \hbar\omega_m b^\dagger b. \quad (6)$$

This vibrational mode interacts with the electronic TLS of the molecule via a polaronic coupling characterised

1 Throughout the article, we use the term *absorption* even though (4) strictly speaking defines the extinction spectrum (i.e. defines the energy lost by the weak probe due to the interaction with the plasmon–exciton system).

Unauthenticated
Download Date | 12/20/19 6:11 PM

by a dimensionless displacement $d=\sqrt{S}$ (S is also known as the Huang–Rhys factor) [50, 53–55]:

$$H_{\mathrm{pol}}=\hbar\omega_{\mathrm{m}}d\sigma^{\dagger}\sigma(b^{\dagger}+b). \tag{7}$$

The total Hamiltonian thus becomes

$$H=H_{\mathrm{J-C}}+H_{\mathrm{vib}}+H_{\mathrm{pol}}, \tag{8}$$

with $H_{\mathrm{J-C}}$ given by (1). As before, we consider that the plasmon resonance is tuned to the electronic transition of the molecule, $\omega_{\mathrm{pl}}=\omega_{\mathrm{eg}}$. Furthermore, besides the losses of the plasmon and the TLS described in the previous section, we incorporate decay processes of the vibrational states via the Lindblad term $\mathcal{L}_b(\rho)=-\frac{\gamma_b}{2}(\{b^{\dagger}b,\rho\}-2b\rho b^{\dagger})$, with γ_b the decay rate of the vibrations.

To illustrate the resonant Raman spectra, we show in Figure 2B the inelastic emission spectra [following (5)] calculated within this full model (black lines) and also for the J-C model neglecting vibrations [(1), red dashed line]. The spectra are plotted for two different strengths of the laser, corresponding to moderate pumping ($\hbar\mathcal{E}=1$ meV) and to excitation near the continuous-laser damage threshold of the sample ($\hbar\mathcal{E}=10$ meV) [5]. In the absence of vibrations, we obtain in both cases the double peak structure that is characteristic of the J-C Hamiltonian before high population states are significantly excited (Figure 1C, D). The main effect of including the vibrations is the emergence of the Stokes line at energy $\hbar\omega_{\mathrm{L}}-\hbar\omega_{\mathrm{m}}$, on top of the J-C (background) spectrum. We also find an anti-Stokes peak at $\hbar\omega_{\mathrm{L}}+\hbar\omega_{\mathrm{m}}$, which is much weaker than the Stokes line, as expected for typical vibration populations $\langle b^{\dagger}b\rangle\ll 1$. A second-order Stokes peak can be also observed at $\hbar\omega_{\mathrm{L}}-2\hbar\omega_{\mathrm{m}}$ for $\hbar\mathcal{E}=1$ meV. Further, for $\hbar\mathcal{E}=10$ meV, as compared to the $\hbar\mathcal{E}=1$ meV case, the background shows qualitatively similar features, but it is four orders of magnitude stronger, i.e. grows as $\propto|\mathcal{E}|^4$. On the other hand, the maximum of the SERS Stokes line grows approximately linearly with the laser intensity $\propto|\mathcal{E}|^2$ as long as the incoherent vibrational population is small. This different scaling with laser intensity decreases the spectral contrast of the Raman signal for the stronger laser, although we observe that for the parameters considered here the main Stokes line clearly dominate the spectrum. We address the strong-intensity effects that go beyond the simple intensity scaling law at the end of the paper.

4 Analytical model

To provide insight into the scattering of light by a molecule, we develop an analytical model describing the Raman process for a relatively simple scenario. We first consider that the electron–phonon coupling, described by the displacement value $d=\sqrt{S}$, is in the low range of possible values, as obtained for rigid molecules [56, 57] ($d\sim 10^{-1}$). We further assume that the laser illumination is not too intense so that the linear response approximation is justified and that the Two-level system is not affected by pure dephasing processes.

The condition of weak electron–vibration coupling, considering that the time scale of the electron–vibration interaction is larger than that of the typically dominant relaxation processes, can be roughly estimated as $\omega_m d<\gamma_a/2$, g. This assumption allows us to separate the full system according to the hierarchy of time scales: on the one hand, the fast-decaying and decohering reservoir part, which consists of the TLS strongly coupled with the plasmon, and on the other hand, the slowly varying part of the system represented by the vibrational mode [51]. This separation of time scales allows for using the Markov approximation and obtaining the effective vibrational dynamics under the influence of the reservoir. The derivation is discussed further in the Supplementary Information and yields the following set of equations:

$$\begin{aligned}\frac{\mathrm{d}}{\mathrm{d}t}\langle b\rangle&=-\mathrm{i}\omega_{\mathrm{m}}\langle b\rangle-\mathrm{i}\omega_{\mathrm{m}}d\langle\sigma^{\dagger}\sigma\rangle_{SS}\\&\quad-(\gamma_b/2+\Gamma_-/2-\Gamma_+/2)\langle b\rangle,\end{aligned} \tag{9}$$

$$\begin{aligned}\frac{\mathrm{d}}{\mathrm{d}t}\langle b^{\dagger}b\rangle&=-\mathrm{i}\omega_{\mathrm{m}}d\langle\sigma^{\dagger}\sigma\rangle_{SS}(\langle b^{\dagger}\rangle-\langle b\rangle)\\&\quad-(\gamma_b+\Gamma_-+\Gamma_+)\langle b^{\dagger}b\rangle+\Gamma_+,\end{aligned} \tag{10}$$

where Γ_+ and Γ_- are, respectively, the effective incoherent pumping and damping rates due to the reservoir. These rates are related to the steady-state reservoir spectral function $\mathcal{J}(s)=\mathrm{Re}\{\int_0^{\infty}\langle\langle\sigma^{\dagger}\sigma(\tau)\sigma^{\dagger}\sigma(0)\rangle\rangle e^{\mathrm{i}s\tau}\mathrm{d}\tau\}$ as follows:

$$\Gamma_-=2\omega_{\mathrm{m}}^2d^2\mathcal{J}(\omega_{\mathrm{m}}) \tag{11}$$

$$\Gamma_+=2\omega_{\mathrm{m}}^2d^2\mathcal{J}(-\omega_{\mathrm{m}}), \tag{12}$$

with the following notation $\langle\langle O_1O_2\rangle\rangle=\langle O_1O_2\rangle-\langle O_1\rangle_{SS}\langle O_2\rangle_{SS}$. In the scheme considered above, the reservoir operators are obtained from the dynamics of the J-C system decoupled from the vibrations.

The steady-state population and coherence follow directly from (9) and (10):

$$\langle b\rangle_{SS}=-\frac{\mathrm{i}\omega_{\mathrm{m}}d\langle\sigma^{\dagger}\sigma\rangle_{SS}}{\gamma_b/2+\Gamma_-/2-\Gamma_+/2+\mathrm{i}\omega_{\mathrm{m}}}, \tag{13}$$

$$\langle b^{\dagger}b\rangle_{SS}=|\langle b\rangle_{SS}|^2+\frac{\Gamma_+}{\gamma_b+\Gamma_-+\Gamma_+}, \tag{14}$$

Unauthenticated
Download Date | 12/20/19 6:11 PM

As we have assumed that the pure dephasing of the TLS is negligible, we can write $\langle\sigma^\dagger\sigma\rangle_{SS} \approx |\langle\sigma\rangle_{SS}|^2$. Next, we decompose the lowering operator of the TLS into its steady-state value $\langle\sigma\rangle_{SS}$ and the fluctuating part with zero mean $\delta\sigma$, as $\sigma = \langle\sigma\rangle_{SS} + \delta\sigma$, and thus we can approximate the population operator as $\sigma^\dagger\sigma \approx |\langle\sigma\rangle_{SS}|^2 + \langle\sigma\rangle_{SS}\delta\sigma^\dagger + \langle\sigma^\dagger\rangle_{SS}\delta\sigma$.

We then transform the dependency of the spectral function $\mathcal{J}(s)$ from the correlation function of the full operator $\langle\langle\sigma^\dagger\sigma(\tau)\sigma^\dagger\sigma(0)\rangle\rangle$ to a simpler dependence with the correlation function $\langle\langle\delta\sigma(\tau)\delta\sigma^\dagger(0)\rangle\rangle = \langle\langle\sigma(\tau)\sigma^\dagger(0)\rangle\rangle$:

$$\begin{aligned}\mathcal{J}(s) &= \mathrm{Re}\{\int_0^\infty \langle\langle\sigma^\dagger\sigma(\tau)\sigma^\dagger\sigma(0)\rangle\rangle e^{is\tau}\mathrm{d}\tau\}\\ &\approx |\langle\sigma\rangle_{SS}|^2\,\mathrm{Re}\{\int_0^\infty \langle\langle\sigma(\tau)\sigma^\dagger(0)\rangle\rangle e^{i(s+\omega_L)\tau}\mathrm{d}\tau\}\\ &= |\langle\sigma\rangle_{SS}|^2 \underbrace{\frac{g^2\frac{\gamma_a}{2}+\frac{\gamma_\sigma}{2}\left[\frac{\gamma_a^2}{4}+(\Delta-s)^2\right]}{g^4-2g^2\left[(\Delta-s)^2-\frac{\gamma_\sigma\gamma_a}{4}\right]+\left[\frac{\gamma_\sigma^2}{4}+(\Delta-s)^2\right]\left[\frac{\gamma_a^2}{4}+(\Delta-s)^2\right]}}_{\equiv\mathcal{J}_0(s)}.\end{aligned} \tag{15}$$

Equation (15) thus can be factorised into two contributions: (i) the coherent population of the TLS, $|\langle\sigma\rangle_{SS}|^2$, which in the limit of low illumination intensity is given by the following expression:

$$\begin{aligned}|\langle\sigma\rangle_{SS}|^2 &\approx \langle\sigma^\dagger\sigma\rangle_{SS}\\ &\approx \frac{g^2|\alpha|^2(\Delta^2+\gamma_a^2/4)}{\Delta^4+(g^2+\gamma_\sigma\gamma_a/4)^2+\Delta^2(\gamma_\sigma^2/4+\gamma_a^2/4-2g^2)},\end{aligned} \tag{16}$$

with $\alpha = \frac{-\mathcal{E}}{\Delta - i\gamma_a/2}$, and (ii) the absorption spectrum of the TLS (that contains the coupling of the TLS with the plasmon), $\mathcal{J}_0(s)$. An approximate version of the latter can be obtained analytically using the quantum regression theorem and considering the low pumping regime. The details of this derivation are given in the Supplementary Information, and the final result appears as the last expression in (15).

In the strong coupling regime, $\mathcal{J}_0(s)$ contains two peaks (i.e. maxima) approximately located at frequencies $s_1^{\mathcal{J}} \approx \Delta + \sqrt{g^2 - (\gamma_\sigma^2+\gamma_a^2)/8}$ and $s_2^{\mathcal{J}} \approx \Delta - \sqrt{g^2 - (\gamma_\sigma^2+\gamma_a^2)/8}$ (assuming a slowly varying numerator). We notice that the double-peaked structure can be resolved only if $g^2 > (\gamma_\sigma^2+\gamma_a^2)/8$.

The expressions for the effective damping (11) and pumping (12), proportional to $\mathcal{J}(s)$, can then be interpreted as being the consequence of a two-step process. First, $|\langle\sigma\rangle_{SS}|^2$ indicates that the pumping laser of frequency ω_L induces coherent population of the molecular excited state, which triggers the Raman process and thus increases Γ_- and Γ_+. In a second stage, the Stokes and anti-Stokes excitations appearing at frequencies $\omega_L \pm \omega_m$ are absorbed and partially emitted to the far field via the resonance of the J-C system, given by $\mathcal{J}_0(s)$ [the emission at the Raman frequencies corresponds to $\mathcal{J}_0(\pm\omega_m)$]. The enhancement of the Stokes scattering at frequency $\omega_L - \omega_m$ leads to the enhancement of the vibrational pumping Γ_+ (a vibrational quantum is created with each emitted Stokes photon), while the anti-Stokes emission at frequency $\omega_L + \omega_m$ contributes to the vibrational damping Γ_-. A similar interpretation has also been shown to be valid for off-resonant SERS [17, 18, 58, 59].

Figure 3 demonstrates the validity of this description. We show in Figure 3A and B two-dimensional D colourmap plots of the incoherent part of the vibrational population, $\langle\langle b^\dagger b\rangle\rangle_{SS} = \langle b^\dagger b\rangle_{SS} - |\langle b\rangle_{SS}|^2$, as a function of the vibrational frequency ω_m and of the detuning Δ of the laser from the plasmon frequency. We display the incoherent part of the population as the coherent part $|\langle b\rangle_{SS}|^2$ represents a constant static displacement of the vibration due to the coherent laser pumping.

The approximate (Figure 3A) and exact (Figure 3B) results are very similar, both exhibiting a clear population maximum for a detuning $\hbar\Delta \approx -100$ meV and a frequency of the vibrational mode $\hbar\omega_m \approx 180$ meV. This maximum can be understood as a consequence of the two-step process described above. Pumping, $|\langle\sigma\rangle_{SS}|^2$, is optimised when the incident laser excites the absorption peaks near the resonant condition $\omega_L \approx \omega_{pl} \pm g$ ($\omega_L \approx \omega_{pl} \pm g$ marked by the vertical green line). On the other hand, the Raman–Stokes process, leading to vibrational pumping, is maximised when the Stokes–Raman line coincides with one of the J-C absorption peaks (red lines, marking the condition $\omega_L - \omega_m \approx \omega_{pl} - g$). Figure 3A and B show that the strongest incoherent vibrational population is indeed achieved when both conditions are fulfilled (region near the intersection of the green and the red line). We remark that for the regime under consideration, $\hbar\mathcal{E} = 1$ meV and temperature $T \approx 0$ K, the enhancement of the anti-Stokes lines does not significantly influence the incoherent vibrational population.

Although the incoherent vibrational populations provide important information about the system dynamics, the quantity typically accessible in experiments is the inelastic Raman emission spectrum [given by (5)]. Using the separation of the system's dynamics into the slow vibration and the fast J-C reservoir, we can isolate the Raman contribution to the scattering spectrum from the fluorescence background (as discussed in Supplementary Information). By doing this, the resulting expressions for the Stokes ($s_{e,S}$) and anti-Stokes ($s_{e,aS}$) emission lines are as follows:

$$\begin{aligned}s_{e,S}(\omega) &= \omega_m^2 d^2 |\langle\sigma\rangle_{SS}|^2 |\mathcal{A}(-\omega_m)|^2\\ &\quad\times 2\mathrm{Re}\{\int_0^\infty \langle\langle b(0)b^\dagger(\tau)\rangle\rangle e^{i(\omega-\omega_L)\tau}\mathrm{d}\tau\},\end{aligned} \tag{17}$$

Unauthenticated
Download Date | 12/20/19 6:11 PM

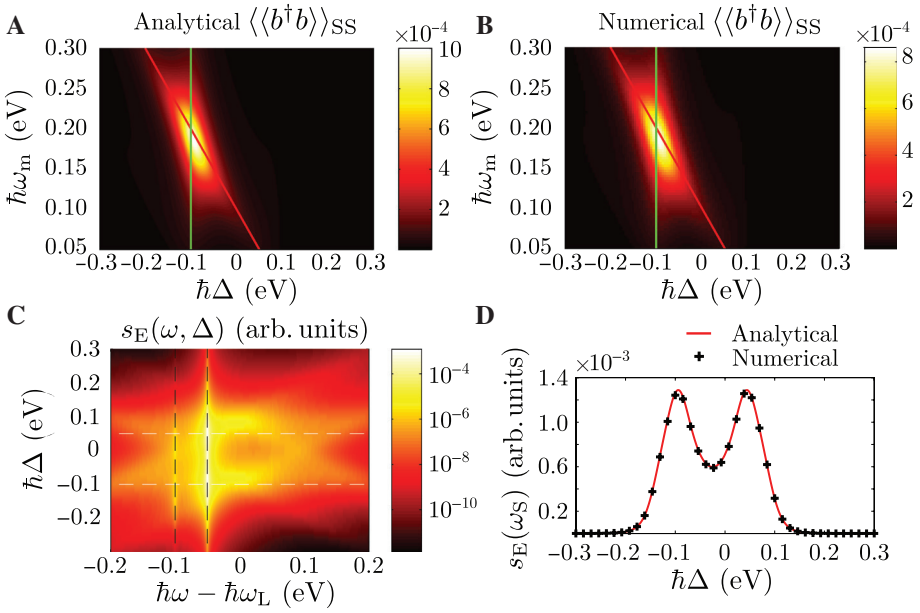

Figure 3: Resonant surface-enhanced Raman scattering for weak illumination ($\hbar\mathcal{E}=1$ meV), no pure dephasing, and weak coupling between the electronic and vibrational levels of the molecule, $d=0.1$.
(A, B) Incoherent population of the vibrational mode under laser excitation as a function of the laser detuning Δ and vibrational frequency ω_m, calculated (A) from the analytical model and (B) from the full numerical calculation. The lines mark the conditions when the frequency of one of the bare J-C absorption peaks coincides with the frequency of the first-order Stokes line (red line) or the incident laser (green line). (C) Numerically calculated surface-enhanced resonant Raman scattering spectra $s_E(\omega, \Delta)$ at emission frequency ω as a function of the plasmon detuning Δ, for a vibrational mode energy $\hbar\omega_m=50$ meV. The black dashed lines mark positions of the first- and second-order Stokes lines. The white dashed lines mark the condition for which either the frequency of the first-order Stokes line or the frequency of the incident laser matches with one of the Jaynes–Cummings peaks. (D) Maximum intensity of the Stokes Raman line (at $\omega=\omega_L-\omega_m$) as a function of the detuning of the incident laser from the plasmon Δ, calculated with the analytical model [(17) (red line)] and with the full numerical model (black crosses). The other parameters used for the calculations in (A–D) are $\hbar\gamma_b=2$ meV, $\hbar\gamma_\sigma=2\times10^{-5}$ eV, $\hbar\gamma_a=150$ meV, $\hbar g=100$ meV, $\hbar\gamma_\phi=0$ eV, $\Delta=\delta$.

$$s_{e,as}(\omega)=\omega_m^2 d^2\,|\langle\sigma\rangle_{SS}|^2\,|\mathcal{A}(\omega_m)|^2 \times 2\mathrm{Re}\{\int_0^\infty\langle\langle b^\dagger(0)b(\tau)\rangle\rangle e^{i(\omega-\omega_L)\tau}d\tau\}, \tag{18}$$

where $|\langle\sigma\rangle_{SS}|^2$ is given by (16), and $|\mathcal{A}|^2$ is the reservoir spectral function that describes the enhancement of the emission of the Raman photons into the far field due to the presence of the J-C system (we assume that the emission from the molecule via the plasmon is much stronger than its direct far-field emission):

$$|\mathcal{A}(s)|^2 = \frac{g^2}{g^4-2g^2[(\Delta-s)^2-\gamma_\sigma\gamma_a/4]+[\gamma_\sigma^2/4+(\Delta-s)^2][\gamma_a^2/4+(\Delta-s)^2]}. \tag{19}$$

This function is double peaked, and for the conditions considered in this article, the peak positions, $s_1^{\mathcal{A}}=\Delta+\sqrt{g^2-(\gamma_\sigma^2+\gamma_a^2)/8}$ and $s_2^{\mathcal{A}}=\Delta-\sqrt{g^2-(\gamma_\sigma^2+\gamma_a^2)/8}$, are similar as $s_1^{\mathcal{J}}$ and $s_2^{\mathcal{J}}$ for the spectral function $\mathcal{J}_0(s)$.

Last, the integrals of the vibrational correlation functions in (17) and (18) represent the emission line shape that can be obtained from the equations describing the dynamics of the vibration coupled with the reservoir [17] (9, 10). Applying the quantum regression theorem to these equations, we obtain

$$\mathrm{Re}\{\int_0^\infty\langle\langle b(0)b^\dagger(t)\rangle\rangle e^{i(\omega-\omega_L)t}\} = \frac{\gamma_{vdp}/2}{(\omega-\omega_L+\omega_m)^2+\gamma_{vdp}^2/4}(1+\langle\langle b^\dagger b\rangle\rangle_{SS}), \tag{20}$$

$$\mathrm{Re}\{\int_0^\infty\langle\langle b^\dagger(0)b(t)\rangle\rangle e^{i(\omega-\omega_L)t}\} = \frac{\gamma_{vdp}/2}{(\omega-\omega_L-\omega_m)^2+\gamma_{vdp}^2/4}\langle\langle b^\dagger b\rangle\rangle_{SS}, \tag{21}$$

with $\gamma_{vdp}=\gamma_b+\Gamma_--\Gamma_+$. The emitted signal (17 and 18) is thus proportional to the efficiency of the excitation of the system, $\propto|\langle\sigma\rangle_{SS}|^2$, and to the emission enhancement due to the coupled TLS plasmon, $|\mathcal{A}(s)|^2$. Furthermore, the anti-Stokes and Stokes lines are proportional to the incoherent population of the vibrations $\langle\langle b^\dagger b\rangle\rangle_{SS}$ and to $1+\langle\langle b^\dagger b\rangle\rangle_{SS}$ [60], respectively, where $\langle\langle b^\dagger b\rangle\rangle_{SS}$ itself is enhanced by the effect of the reservoir on the excitation and emission process (11–15). The line width of the Raman peaks is

Unauthenticated
Download Date | 12/20/19 6:11 PM

finally given by the interplay between the damping rates, γ_b together with Γ_-, both broadening the peak, and the pumping rate Γ_+ that narrows the peak. These properties again mirror the behaviour that has been discussed for off-resonant Raman [16–18], except for the existence of a more complex reservoir.

Figure 3C and D illustrate the behaviour of the resulting Raman emission for a vibrational mode of energy $\hbar\omega_m = 50$ meV and $d = \sqrt{S} = 0.1$. We first show in Figure 3C the emission spectra obtained from the numerical solution of the full system [Hamiltonian in (8) and corresponding loss terms], as a function of the detuning Δ of the laser from the plasmon frequency. The inelastic emission can be split into two components, the emission resulting from the resonance fluorescence of the J-C system and the Raman emission yielding the vibrational lines. The former is present in the emission spectra of Figure 3C as a broad background symmetrical around the zero detuning $\hbar\Delta = 0$ meV, in agreement with previous studies [28, 48]. The strong Raman–Stokes line is also clearly distinguished on top of the background at $\omega_L - \omega_m$, accompanied by a second-order Stokes transition line (not described by the analytical model that accounts only for the first-order transition) at $\omega_L - 2\omega_m$ and a very weak anti-Stokes line at $\omega_L + \omega_m$.

To better analyse the Δ dependence of the Raman signal and further test the validity of our model, we focus in Figure 3D on the maximum of the Stokes line, which we plot as a function of the laser detuning Δ as calculated from the full numerical model (black dots) and as given by the analytical expression in (17) (red line). The agreement between the two is excellent. We observe a double-peaked structure that is, however, not symmetric with respect to $\Delta = 0$, but with the central minimum blue-detuned by 25 meV. This blue detuning can be understood as the result of having to optimise the product of the enhancement at the excitation ω_L and emission $\omega_L - \omega_m$ frequencies, as given by $|\langle\sigma\rangle_{SS}|^2$ and $|\mathcal{A}(s)|^2$, respectively (assuming that the incoherent vibrational population remains small $\langle\langle b^\dagger b\rangle\rangle_{SS} \ll 1$). The individual contributions of $|\langle\sigma\rangle_{SS}|^2$ and $|\mathcal{A}(s)|^2$ are shown in Figure S1 of the Supplementary Information.

5 Effect of strong electron–vibration coupling

We now consider scenarios that go beyond the assumptions of the previous section. Up to now, we have assumed that the coupling between the molecular vibrational and electronic states, characterised by the dimensionless displacement d (the Huang–Rhys parameter $S = d^2$), was weak. However, when the interaction becomes stronger, and thus the time scale of the coupling between the electronic TLS and the phonon is shortened, the dynamics of the J-C system coupled to the vibrational mode are no longer separable as a slow vibrational dynamics driven by the fast relaxing reservoir. For large d, we thus cannot apply the description developed in the previous section, and we use full numerical solutions to obtain the response of the system.

We show in Figure 4A and B the maps of the incoherent vibrational population for large electron–vibration couplings (A) $d = 0.5$ and (B) $d = 1$ (B) as a function of laser detuning and vibrational frequency. The lines in Figure 4A and B have the same meaning as in Figure 3A and B, indicating the detuning Δ at which the first-order Stokes line (red line) or the incident laser frequency (green line) is tuned to the position of one of the absorption peaks of the J-C system. For $d = 0.5$ (Figure 4A), the strongest vibrational pumping appears approximately when both conditions are met and the lines cross, similarly as for low $d = 0.1$ (Figure 3A and B). Nonetheless, while for $d = 0.1$ a single clear peak was observed, two close maxima start to emerge near this optimal condition for $d = 0.5$. The effect of large electron–vibration coupling is more apparent in the case with $d = 1$ (Figure 4B). In this situation, the dependence of the incoherent vibrational population on the vibrational frequency and detuning becomes very complex as it involves the influence of higher-order vibronic transitions.

Next we consider the emission spectra for Figure 4C moderate ($d = 0.5$) and Figure 4D strong ($d = 1$) electron–vibration coupling when two values of pumping amplitude, $\hbar\mathcal{E} = 1$ meV and 10 meV, are considered. The spectra for weak electron–vibration coupling ($d = 0.1$) are shown in Figure 2B. For $d = 0.5$, the results for both illumination intensities show a clear lower-order Stokes peak at $\omega = \omega_L - \omega_m$ and a weaker anti-Stokes peak at $\omega = \omega_L + \omega_m$. A series of higher-order Stokes peaks is observed at $\omega = \omega_L - n\omega_m$ (with $n = 2, 3, 4$), much stronger than in the case of the spectra calculated for $d = 0.1$. Increasing the displacement d of the excited state vibrations naturally leads to larger overlaps among vibrational wave functions belonging to different numbers of vibrational excitations, thus facilitating higher-order Raman transitions that yield intense higher-order Raman peaks. This can be observed most clearly in Figure 4D, where, for $d = 1$, particularly intense Raman peaks of higher orders emerge on both the Stokes and anti-Stokes sides of the spectra, most notably for $\hbar\mathcal{E} \approx 10$ meV.

Unauthenticated
Download Date | 12/20/19 6:11 PM

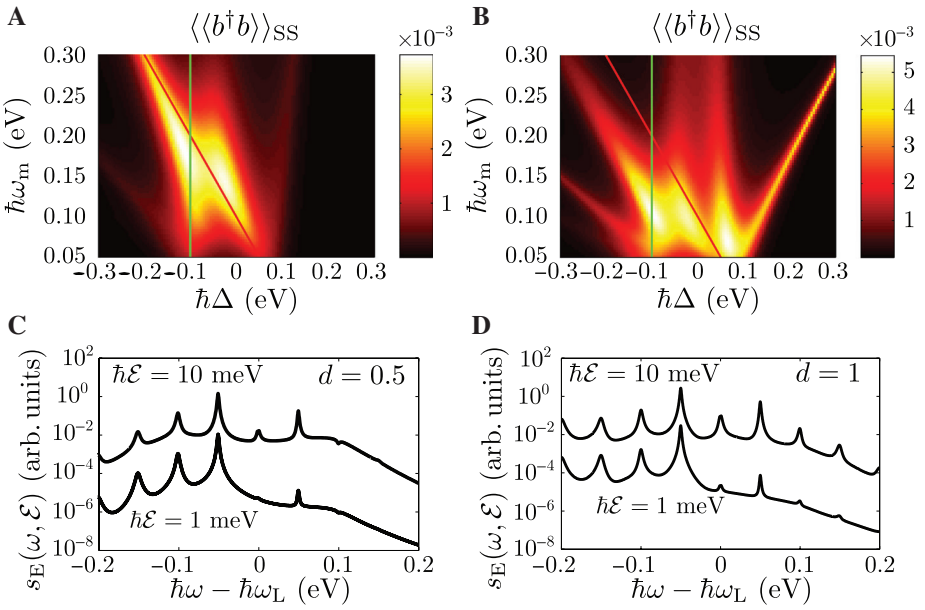

Figure 4: Effect of electron–vibration coupling on resonant surface-enhanced Raman scattering (SERS).
(A, B) Incoherent population of the vibrational mode as a function of the laser detuning Δ and vibrational frequency $\omega_{\rm m}$ for an electron–vibration coupling (Huang–Rhys) parameter (A) $d = \sqrt{S} = 0.5$ and (B) $d = 1$. Results are obtained numerically. In both cases, $\hbar\mathcal{E} = 1$ meV, and there is no pure dephasing. The straight lines mark the conditions when the peak frequency of one of the bare J-C absorption peaks coincides with the frequency of the incident laser (green line) or with the first-order Stokes line (red line). (C, D) SERS spectra of a molecule supporting a single vibrational mode of energy $\hbar\omega_{\rm m} = 50$ meV, for two values of the electron–vibration coupling, (C) $d = 0.5$ and (D) $d = 1$, and illumination intensity $\hbar\mathcal{E} = 1$ meV and 10 meV. The other parameters used for all the calculation are as follows: $\hbar\gamma_b = 2$ meV, $\hbar\gamma_\sigma = 2\times10^{-5}$ eV, $\hbar\gamma_a = 150$ meV, $\hbar g = 100$ meV, $\hbar\gamma_\phi = 0$ eV, $\Delta = \delta$.

6 Effect of pure dephasing

So far, we have assumed negligible dephasing. This is the case for optimised experiments at low temperature, but for a typical situation at finite temperature, the electronic transition is subjected to a large pure dephasing rate, γ_ϕ, due to interactions with the environment. In molecules decoupled from the plasmonic cavity, pure dephasing introduces a loss of coherence between the states of the TLS but without directly inducing the decay of the excited state [49]. A careful analysis of the microscopic dephasing mechanism shows that when the polaritonic states $|N, \pm\rangle$ are formed, the interaction of the system with the originally purely dephasing reservoir leads to novel incoherent mechanisms including the energy transfer from the upper polariton states $|N, +\rangle$ to the lower ones $|N, -\rangle$ within the same manifold [61, 62]. In the following, we again consider that the system is illuminated by a weak laser, and hence only the single-excitation manifold containing the states $|1, \pm\rangle \equiv |\pm\rangle$ is important for the description of the inelastic light emission from the polaritons.

We implement the dephasing processes by incorporating the following Lindblad terms in the master equation:

$$\mathcal{L}_{\sigma_{-++}}(\rho) = -\gamma_\phi(\{\sigma_{-++}\sigma_{-++}, \rho\} - 2\sigma_{-++}\rho\sigma_{-++}) \tag{22}$$

$$\mathcal{L}_{\sigma_{-+}}(\rho) = -\frac{\gamma_{\sigma_{-+}}}{2}(\{\sigma^\dagger_{-+}\sigma_{-+}, \rho\} - 2\sigma_{-+}\rho\sigma^\dagger_{-+}), \tag{23}$$

where $\sigma_{-++} = |+\rangle\langle+| + |-\rangle\langle-|$ and $\sigma_{-+} = |-\rangle\langle+|$. We neglect any further incoherent processes such as the energy transfer from the lower to the upper polariton as we assume that they are less effective [15, 62]. We further set $\hbar\gamma_{\sigma_{-+}} = 40$ meV whenever we consider $\hbar\gamma_\phi \neq 0$ eV, a rate that leads to relatively strong transfer of populations towards the lower polaritonic state via the vibrational reservoir of the molecule [63, 64].

To illustrate the effect of dephasing, we start by plotting the absorption, $s_{\rm A}(\omega)$ (Figure 5A), and emission, $s_{\rm E}(\omega)$ (Figure 5B), spectra for the bare plasmon–exciton J-C system, without vibrations. In both cases, we set $\hbar\mathcal{E} = 1$ meV, and we show results for $\hbar\gamma_\phi = 0$ meV, 10 meV, and 50 meV. For clarity, the spectra are vertically shifted. When the dephasing is increased, we observe a clear broadening of the polariton peaks in the absorption spectrum (Figure 5A), which is larger for the upper

Unauthenticated
Download Date | 12/20/19 6:11 PM

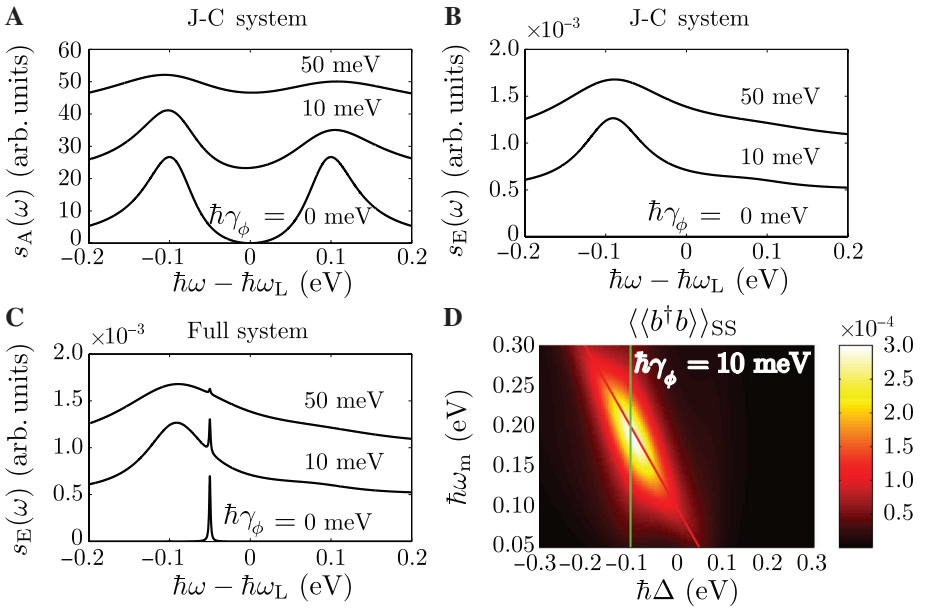

Figure 5: Effect of pure dephasing for weak illumination ($\hbar\mathcal{E}=1$ meV) and electron–vibration coupling $d=0.1$.
(A) Absorption spectra and (B) emission spectra for the simple J-C system in Figure 1, displayed for three different values of pure dephasing, $\hbar\gamma_\phi=0$ meV, 10 meV, and 50 meV, pumped by monochromatic illumination tuned to the plasmonic resonance $\hbar\Delta=\hbar\omega_{pl}-\hbar\omega_L=0$ eV. (C) Emission spectra of the full molecule–plasmon system (sketched in Figure 2A) including the vibrational mode of frequency $\hbar\omega_m=50$ meV, for $\hbar\Delta=0$ eV and the same γ_ϕ values as in (A, B). The spectra in (A–C) are offset from each other by a constant value of $s_A=20$ in (A) and $s_E=0.5\times10^{-3}$ in (B, C). (D) Incoherent populations of the vibrational mode as a function of detuning and vibrational frequency for pure dephasing $\hbar\gamma_\phi=10$ meV. The lines drawn into the colour maps mark the detuning Δ for which the first-order Stokes line (red line) or the incident laser (green line) coincides with one of the bare J-C absorption peaks. The other parameters used for all the calculations in (A–D) are $\hbar\gamma_b=2$ meV, $\hbar\gamma_\sigma=2\times10^{-5}$ eV, $\hbar\gamma_a=150$ meV, $\hbar g=100$ meV, $\hbar\Delta=\hbar\delta=0$ eV.

polaritonic peak due to the population transfer given by terms in (23).

The dephasing-induced broadening also affects the J-C emission spectra $s_E(\omega)$ shown in Figure 5B for $\hbar\mathcal{E}=1$ meV and $\hbar\Delta=0$ eV. When the dephasing is switched on, there appears a strong inelastic contribution to the light emission originating predominantly from the lower polariton branch, as the upper branch is efficiently depopulated by the incoherent energy transfer. Without dephasing, the emission spectrum practically vanishes as the incoherent population of the polaritons is low.

Finally, we turn on the interaction between the molecular electronic and vibrational levels and calculate the effect of dephasing on the emission spectra of the complete system. The resulting emission spectra are shown in Figure 5C for the same parameters as the emission spectra of the bare polaritons in Figure 5B and for $d=0.1$, $\hbar\omega_m=50$ meV and $\hbar g=100$ meV. All of the spectra feature a sharp Stokes–Raman peak at the frequency $\omega_L-\omega_m$, which for $\hbar\gamma_\phi=10$ meV and 50 meV is accompanied by the broad and intense fluorescence background already discussed in Figure 5B. Particularly for $\hbar\gamma_\phi=50$ meV, the background overwhelms the relatively weak SERS signal. For no dephasing, this background is strongly reduced and becomes negligible in comparison with the Raman peak.

For completeness, we show in Figure 5D the incoherent population of the vibrational level for the same parameter $d=0.1$, pumping amplitude $\hbar\mathcal{E}=1$ meV, and for $\hbar\gamma_\phi=10$ meV. The results as a function of laser detuning and vibrational frequency can be compared with those in Figure 3A, where we plotted the same results except that we adopted $\hbar\gamma_\phi=0$ eV there. As expected, the most noticeable feature introduced by dephasing is the larger width of the displayed features and the lower populations.

7 Effect of strong illumination

We now consider the situation where the intensity of the incident laser is strong, while the electron–vibration coupling is assumed to be weak, and in the absence of pure dephasing. An intense laser populates the different manifolds of the J-C ladder and thus leads to nonlinear effects in the resonant SERRS signal that were not considered in our weak-illumination expressions. A full analytical treatment of this situation is very challenging, but we can still gain

Unauthenticated
Download Date | 12/20/19 6:11 PM

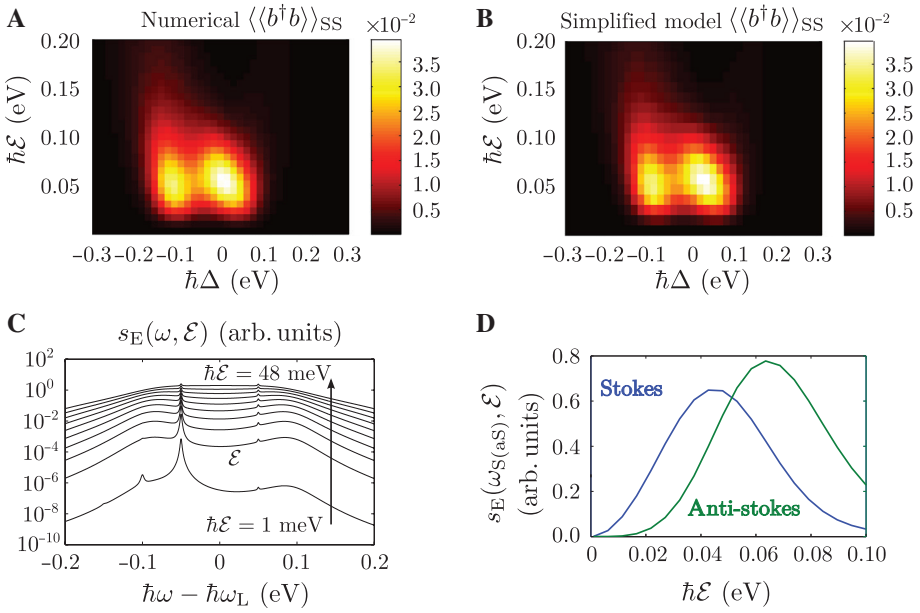

Figure 6: Nonlinear resonant surface-enhanced Raman scattering (SERS) response for strong laser illumination. (A, B) Incoherent population of a vibrational mode of energy $\hbar\omega_m = 50$ meV as a function of the laser detuning and pumping amplitude $\mathcal{E}$ calculated from (A) the full numerical model and (B) the simplified model. The vibrations are weakly coupled to the electronic states ($d = 0.1$), and there is no pure dephasing. (C, D) Evolution of the SERS emission with pumping amplitude ($\mathcal{E}$), calculated numerically for a single vibrational mode of energy $\hbar\omega_m = 50$ meV that is weakly coupled to the electronic states ($d = 0.1$) (C) Emission spectra as a function of $\mathcal{E}$ for detuning of the incident laser $\hbar\Delta = 0$ eV. (D) Maximum intensity of the Stokes (blue line) and anti-Stokes (green line) Raman line as a function of $\mathcal{E}$ [shown in (C) for up to $\hbar\mathcal{E} = 48$ meV]. To obtain the value of the Raman peaks, we first subtracted the background, defined as the inelastic emission of the J-C system. The other parameters used for all calculations are as follows: $\hbar\gamma_b = 2$ meV, $\hbar\gamma_\sigma = 2\times10^{-5}$ eV, $\hbar\gamma_a = 150$ meV, $\hbar g = 100$ meV, $\hbar\gamma_\phi = 0$ eV, $\Delta = \delta$.

insight into the vibrational dynamics, assuming the same separation of time scales as discussed before, by inserting the numerically calculated reservoir spectral function $\mathcal{J}(s)$ into the expression of the decay and pumping rates (11 and 12) and then using these values in the rate equations of the vibrations (9 and 10) to obtain the steady-state value of the vibrational population (14). We complement this simplified semianalytical approach by full numerical calculations. For simplicity, we continue using the rotation wave approximation, although for the strongest laser considered, a correction may be necessary.

We plot in Figure 6 the incoherent vibrational population as a function of the amplitude $\mathcal{E}$ and detuning Δ of the illuminating laser, obtained using the full-numerical (Figure 6A) and the semianalytical (Figure 6B) approach, and for $d = 0.1$, $\hbar\omega_m = 50$ meV and $\hbar g = 100$ meV. The excellent agreement between the two supports the assumption that the use of very intense laser illumination does not invalidate the separation of the system into the slowly evolving vibrations and the fast J-C reservoir.

More strikingly, the incoherent population is strongly nonlinear with respect to the intensity, $\propto|\mathcal{E}|^2$, of the incident laser. For weak illumination, we are in the linear regime, where the incoherent population shows local maxima for two different moderate detunings, as obtained from (14), together with (11), (12), and (15), analogously to the results in the previous section. The incoherent population of these peaks initially grows when increasing $\mathcal{E}$ as more energy is pumped into the system, but for a certain laser intensity, the incoherent population reaches a maximum and starts to decay. We attribute this behaviour to the underlying nonlinearity of the J-C system due to the uneven spacing of the energy levels sketched in Figure 1B.

An intense illumination can also affect very strongly the SERRS spectra measured in an experiment. We study this situation with use of the full-numerical calculations and, as an example, we show the inelastic emission spectra as a function of pumping amplitude $\mathcal{E}$ for zero detuning $\Delta = 0$ (Figure 6C, notice the logarithmic scale). The calculated emission spectra can still be regarded as a combination of the resonance fluorescence background and the Raman lines. For low illumination intensities, the spectra in Figure 6C feature a clear Raman–Stokes peak at emission frequency $\omega = \omega_L - \omega_m$ with a strength that is significantly stronger than that of the background. One can also distinguish a second-order Stokes peak at $\omega = \omega_L - 2\omega_m$ and the anti-Stokes peak at $\omega = \omega_L + \omega_m$. As the intensity of the laser is increased, but still sufficiently small, the strength

Unauthenticated
Download Date | 12/20/19 6:11 PM

of both the background and Raman peaks increases, with the latter remaining clearly visible. In contrast, for very large laser intensities $\hbar\mathcal{E} \gtrapprox 100$ meV, the amplitude of the Raman peaks is reduced, and the spectrum is fully dominated by the background.

The laser intensity also affects the spectral shape of the background. For example, the two broad background peaks in Figure 6C for $\hbar\mathcal{E}=1$ meV become a single broad flat feature for $\hbar\mathcal{E}=48$ meV. Therefore, the laser intensity does not simply scale the emission spectra by a frequency-independent factor, but it changes the overall spectral shape and affects the relative weights of the Raman lines and the background.

Finally, we highlight in Figure 6D the nonlinear dependence of the maximum of the SERS signal on the incident laser amplitude by plotting the background-free maxima of the Raman–Stokes (blue line) and anti-Stokes (green line) lines. The background that we subtract from the total signal corresponds to the inelastic emission spectrum of the J-C system uncoupled from the vibrational modes. The results show that the intensity dependence of the Stokes and anti-Stokes amplitude resembles the result for the incoherent vibrational populations (Figure 6A and B), with a broad maximum that peaks at an optimal pumping amplitude $\mathcal{E}$. Interestingly, the optimal illumination-field amplitude is different for the Stokes and the anti-Stokes lines. The maximum of the anti-Stokes line appears at roughly the pumping amplitude $\hbar\mathcal{E}\approx 70$ meV, while the Stokes emission peaks are maximised at lower powers $\hbar\mathcal{E}\approx 45$ meV.

We notice that such illumination strengths correspond to very intense lasers that can destroy the sample [the sample damage threshold estimated in [5] $W=10^2$ μW/μm^2 ($W\propto\mathcal{E}^2$), can be roughly expressed in terms of the pumping amplitude as $\hbar\mathcal{E}\approx 10$ meV] and may require pulsed illumination [19]. Further, for such strong lasers, a more rigorous calculation will require going beyond the rotating-wave approximation used in this article, and other effects (anharmoniticies of the vibrations, excitation of other electronic states) can become important.

8 Outlook and conclusions

We have studied the resonant SERS process for a system where the molecular exciton is strongly coupled to a single plasmonic mode, forming thus a set of polaritons that interact with a vibrational mode of the same molecule. To bring insight into the underlying physical mechanisms behind this inelastic process in this system, we have first developed an intuitive analytical description of the vibrational pumping and associated Raman scattering for weak-illumination conditions $\mathcal{E}$, weak electron–phonon coupling, and no pure dephasing. The analytical results match the full numerical calculations very well and allow for a simple interpretation of the vibrational pumping mechanism as a two-step process that is similar to the mechanism discussed for nonresonant SERS [16–18, 58] and SERRS in the weak-coupling regime [28] but for a more complex reservoir. In the first step, the amplitude of incident light excites a coherent population of the electronic state in the molecule. In a second step, the Raman–Stokes excitation is spontaneously transferred into the J-C system formed by the coupling of the plasmon and the electronic TLS. This excitation is then either absorbed or re-emitted into the far field.

We have also studied more complex situations. We first considered the influence of two intrinsic parameters of the system, namely, the electron–phonon coupling, $S=d^2$, and the pure dephasing, γ_ϕ. Larger values of d promote higher-order vibrational transitions and generally increase the interaction strength between the electronic and vibrational states of the molecule, leading to the breakdown of the simple reservoir-system picture introduced for small d and to the emergence of higher-order Raman peaks in the emission spectra. On the other hand, pure dephasing reduces the efficiency of vibrational pumping, leading to smaller final incoherent vibrational populations, and thus diminishes the intensity of vibrational Raman peaks in the inelastic emission spectra. Dephasing also significantly broadens and enhances the fluorescence background. As a consequence of the weaker lines and stronger background, the visibility of the Raman lines becomes considerably smaller, which complicates the realisation of SERRS experiments.

Last, we have addressed the effect of increasing the intensity of the illumination. We have shown that the interpretation of the SERRS process as a two-step enhancement process as described above remains valid, but the system becomes strongly nonlinear due to the nonhomogeneous separation of the polaritonic levels of the J-C system (J-C ladder). The strong nonlinear response of the two-level transition likely stands behind the counterintuitive finding of a maximum of the incoherent vibrational population and SERRS signal for a particular value of the pumping laser amplitude.

Acknowledgements: The authors acknowledge project FIS2016-80174-P from the Spanish Ministry of Education, H2020-FETOPEN project "THOR" Nr. 829067 from the European Commission, grant IT1164-19 for consolidated groups of the University from the Basque Government, and project PI2017-30 of the Departamento de Educación, Política Lingüística y Cultura of the Basque Government.

Unauthenticated
Download Date | 12/20/19 6:11 PM

References

[1] Kristensen PT, Hughes S. Modes and mode volumes of leaky optical cavities and plasmonic nanoresonators. ACS Photonics 2013;1:2–10.

[2] Koenderink AF. On the use of Purcell factors for plasmon antennas. Opt Lett 2010;35:4208–10.

[3] Sauvan C, Hugonin JP, Maksymov IS, Lalanne P. Theory of the spontaneous optical emission of nanosize photonic and plasmon resonators. Phys Rev Lett 2013;110:237401.

[4] Tame MS, McEnery K, Özdemir Ş, Lee J, Maier S, Kim M. Quantum plasmonics. Nat Phys 2013;9:329–40.

[5] Benz F, Schmidt MK, Dreismann A, et al. Single-molecule optomechanics in "picocavities". Science 2016;354:726–9.

[6] Chikkaraddy R, Turek VA, Kongsuwan N, et al. Mapping nanoscale hotspots with single-molecule emitters assembled into plasmonic nanocavities using DNA origami. Nano Lett 2018;18:405–11.

[7] Xu H, Bjerneld EJ, Käll M, Börjesson L. Spectroscopy of single hemoglobin molecules by surface enhanced Raman scattering. Phys Rev Lett 1999;83:4357–60.

[8] Moskovits M. Surface-enhanced Raman spectroscopy: a brief retrospective. J Raman Spectrosc 2005;36:485–96.

[9] Haes AJ, Haynes CL, McFarland AD, Schatz GC, Van Duyne RP, Zou S. Plasmonic materials for surface-enhanced sensing and spectroscopy. MRS Bull 2005;30:368–75.

[10] Stiles PL, Dieringer JA, Shah NC, Duyne RPV. Surface-enhanced Raman spectroscopy. Annu Rev Anal Chem 2008;1:601–26.

[11] Galloway CM, Etchegoin PG, Le Ru EC. Ultrafast nonradiative decay rates on metallic surfaces by comparing surface-enhanced Raman and fluorescence signals of single molecules. Phys Rev Lett 2009;103:063003.

[12] Tong L, Xu H, Käll M. Nanogaps for SERS applications. MRS Bull 2014;39:163–8.

[13] Restrepo J, Ciuti C, Favero I. Single-polariton optomechanics. Phys Rev Lett 2014;112:013601.

[14] Roelli P, Galland C, Piro N, Kippenberg TJ. Molecular cavity optomechanics as a theory of plasmon-enhanced Raman scattering. Nat Nanotechnol 2016;11:164–9.

[15] del Pino J, Feist J, García-Vidal FJ. Signatures of vibrational strong coupling in Raman scattering. J Phys Chem C 2015;119:29132–7.

[16] Schmidt MK, Esteban R, González-Tudela A, Giedke G, Aizpurua J. Quantum mechanical description of Raman scattering from molecules in plasmonic cavities. ACS Nano 2016;10:6291–8.

[17] Kamandar Dezfouli M, Hughes S. Quantum optics model of surface-enhanced Raman spectroscopy for arbitrarily shaped plasmonic resonators. ACS Photonics 2017;4:1245–56.

[18] Schmidt MK, Esteban R, Benz F, Baumberg JJ, Aizpurua J. Linking classical and molecular optomechanics descriptions of SERS. Faraday Discuss 2017;205:31–65.

[19] Lombardi A, Schmidt MK, Weller L, et al. Pulsed molecular optomechanics in plasmonic nanocavities: from nonlinear vibrational instabilities to bond-breaking. Phys Rev X 2018;8:011016.

[20] Dezfouli MK, Gordon R, Hughes S. Molecular optomechanics in the anharmonic cavity-QED regime using hybrid metal-dielectric cavity modes. ACS Photonics 2019;6:1400–8.

[21] Ashrafi SM, Malekfar R, Bahrampour AR, Feist J. Optomechanical heat transfer between molecules in a nanoplasmonic cavity. Phys Rev A 2019;100:013826.

[22] Aspelmeyer M, Kippenberg TJ, Marquardt F. Cavity optomechanics. Rev Mod Phys 2014;86:1391–452.

[23] Kneipp K, Wang Y, Kneipp H, Itzkan II, Dasari RR, Feld MS. Population pumping of excited vibrational states by spontaneous surface-enhanced Raman scattering. Phys Rev Lett 1996;76:2444–7.

[24] Haslett TL, Tay L, Moskovits M. Can surface-enhanced Raman scattering serve as a channel for strong optical pumping? J Chem Phys 2000;113:1641–6.

[25] Brolo AG, Sanderson AC, Smith AP. Ratio of the surface-enhanced anti-Stokes scattering to the surface-enhanced Stokes-Raman scattering for molecules adsorbed on a silver electrode. Phys Rev B 2004;69:045424.

[26] Maher RC, Cohen LF, Etchegoin P, Hartigan HJN, Brown RJC, Milton MJT. Stokes/anti-Stokes anomalies under surface enhanced Raman scattering conditions. J Chem Phys 2004;120:11746–53.

[27] Le Ru EC, Etchegoin PG. Vibrational pumping and heating under SERS conditions: fact or myth? Faraday Discuss 2006;132:63–75.

[28] Neuman T, Esteban R, Giedke G, Schmidt MK, Aizpurua J. Quantum description of surface-enhanced resonant Raman scattering within a hybrid-optomechanical model. Phys Rev A 2019;100:043422.

[29] Galperin M, Ratner MA, Nitzan A. Raman scattering in current-carrying molecular junctions. J Chem Phys 2009;130:144109.

[30] Ramos T, Sudhir V, Stannigel K, Zoller P, Kippenberg TJ. Nonlinear quantum optomechanics via individual intrinsic two-level defects. Phys Rev Lett 2013;110:193602.

[31] Dintinger J, Klein S, Bustos F, Barnes WL, Ebbesen TW. Strong coupling between surface plasmon-polaritons and organic molecules in subwavelength hole arrays. Phys Rev B 2005;71:035424.

[32] Bellessa J, Bonnand C, Plenet JC, Mugnier J. Strong coupling between surface plasmons and excitons in an organic semiconductor. Phys Rev Lett 2004;93:036404.

[33] Wiederrecht GP, Wurtz GA, Hranisavljevic J. Coherent coupling of molecular excitons to electronic polarizations of noble metal nanoparticles. Nano Lett 2004;4:2121–5.

[34] Fofang NT, Park T-H, Neumann O, Mirin NA, Nordlander P, Halas NJ. Plexcitonic nanoparticles: plasmon – exciton coupling in nanoshell-J-aggregate complexes. Nano lett 2008;8:3481–7.

[35] Würthner F, Kaiser TE, Saha-Möller CR. J-aggregates: from serendipitous discovery to supramolecular engineering of functional dye materials. Angew Chem 2011;50:3376–410.

[36] Zengin G, Wersäll M, Nilsson S, Antosiewicz TJ, Käll M, Shegai T. Realizing strong light-matter interactions between single-nanoparticle plasmons and molecular excitons at ambient conditions. Phys Rev Lett 2015;114:157401.

[37] Ebbesen TW. Hybrid light–matter states in a molecular and material science perspective. Acc Chem Res 2016;49:2403–12.

[38] Melnikau D, Esteban R, Savateeva D, et al. Rabi splitting in photoluminescence spectra of hybrid systems of gold nanorods and J-Aggregates. J Phys Chem Lett 2016;7:354–62.

[39] Wersäll M, Cuadra J, Antosiewicz TJ, Balci S, Shegai T. Observation of mode splitting in photoluminescence of individual plasmonic nanoparticles strongly coupled to molecular excitons. Nano Lett 2017;17:551–8.

Unauthenticated
Download Date | 12/20/19 6:11 PM

[40] Thompson RJ, Rempe G, Kimble HJ. Observation of normal-mode splitting for an atom in an optical cavity. Phys Rev Lett 1992;68:1132–5.
[41] Delga A, Feist J, Bravo-Abad J, Garcia-Vidal FJ. Quantum emitters near a metal nanoparticle: strong coupling and quenching. Phys Rev Lett 2014;112:253601.
[42] Chikkaraddy R, de Nijs B, Benz F, et al. Single-molecule strong coupling at room temperature in plasmonic nanocavities. Nature 2016;535:127–30.
[43] Trügler A, Hohenester U. Strong coupling between a metallic nanoparticle and a single molecule. Phys Rev B 2008;77:115403.
[44] George J, Wang S, Chervy T, et al. Ultra-strong coupling of molecular materials: spectroscopy and dynamics. Faraday Discuss 2015;178:281–94.
[45] Santhosh K, Bitton O, Chuntonov L, Haran G. Vacuum Rabi splitting in a plasmonic cavity at the single quantum emitter limit. Nat Commun 2016;7:ncomms11823.
[46] Groß H, Hamm JM, Tufarelli T, Hess O, Hecht B. Near-field strong coupling of single quantum dots. Sci Adv 2018;4:eaar4906.
[47] Leng H, Szychowski B, Daniel M-C, Pelton M. Strong coupling and induced transparency at room temperature with single quantum dots and gap plasmons. Nat Commun 2018;9:4012.
[48] del Valle E, Laussy FP, Tejedor C. Luminescence spectra of quantum dots in microcavities. II. Fermions. Phys Rev B 2009;79:235326.
[49] González-Tudela A, del Valle E, Cancellieri E, Tejedor C, Sanvitto D, Laussy F. Effect of pure dephasing on the Jaynes-Cummings nonlinearities. Opt Express 2010;18:7002–9.
[50] Ćwik JA, Kirton P, De Liberato S, Keeling J. Excitonic spectral features in strongly coupled organic polaritons. Phys Rev A 2016;93:033840.
[51] Breuer H-P, Petruccione F. Open quantum electrodynamics. The theory of open quantum systems. Oxford University Press, New York, 2003.
[52] Fink J, Göppl M, Baur M, et al. Climbing the Jaynes–Cummings ladder and observing its nonlinearity in a cavity QED system. Nature 2008;454:315–8.
[53] Klessinger M, Michl J. Excited states and photo-chemistry of organic molecules. Wiley, NY, USA, 1995.
[54] May V, Kühn O. Charge and energy transfer dynamics in molecular systems. John Wiley & Sons, Weinheim, Germany, 2011.
[55] Herrera F, Spano FC. Absorption and photoluminescence in organic cavity QED. Phys Rev A 2017;95:053867.
[56] Hakala TK, Toppari JJ, Kuzyk A, et al. Vacuum Rabi splitting and strong-coupling dynamics for surface-plasmon polaritons and rhodamine 6G molecules. Phys Rev Lett 2009;103:053602.
[57] Kéna-Cohen S, Davanço M, Forrest SR. Strong Exciton-Photon coupling in an organic single crystal microcavity. Phys Rev Lett 2008;101:116401.
[58] Maher RC, Cohen LF, Le Ru EC, Etchegoin PG. A study of local heating of molecules under Surface Enhanced Raman Scattering (SERS) conditions using the anti-Stokes/Stokes ratio. Faraday Discuss 2006;132:77–83.
[59] Le Ru EC, Galloway C, Etchegoin PG. On the connection between optical absorption/extinction and SERS enhancements. Phys Chem Chem Phys 2006;8:3083–7.
[60] Maher RC, Etchegoin PG, Le Ru EC, Cohen LF. A conclusive demonstration of vibrational pumping under surface enhanced Raman scattering conditions. J Phys Chem B 2006;110:11757–60.
[61] del Pino J, Feist J, García-Vidal FJ. Quantum theory of collective strong coupling of molecular vibrations with a microcavity mode. New J Phys 2015;17:053040.
[62] Neuman T, Aizpurua J. Origin of the asymmetric light emission from molecular exciton–polaritons. Optica 2018;5:1247–55.
[63] Schwartz T, Hutchison JA, Léonard J, Genet C, Haacke S, Ebbesen TW. Polariton dynamics under strong light-molecule coupling. Chem Phys Chem 2013;14:125–31.
[64] Canaguier-Durand A, Genet C, Lambrecht A, Ebbesen TW, Reynaud S. Non-Markovian polariton dynamics in organic strong coupling. Eur Phys J D 2015;69:24.

Supplementary Material: The online version of this article offers supplementary material (https://doi.org/10.1515/nanoph-2019-0336).
Article note: The data used in this paper can be found in http://hdl.handle.net/10261/196160.

Unauthenticated
Download Date | 12/20/19 6:11 PM